AIAA JOURNAL
Vol. 45, No. 8, August 2007

Nonsinusoidal Path Optimization of a Flapping Airfoil

Mustafa Kaya* and Ismail H. Tuncer†
Middle East Technical University, 06531 Ankara, Turkey

DOI: 10.2514/1.29478

The path of a flapping airfoil undergoing a combined, nonsinusoidal pitching and plunging motion is optimized for maximum thrust and/or propulsive efficiency. The nonsinusoidal, periodic flapping motion is described using nonuniform rational B splines. A gradient based algorithm is then employed for the optimization of the nonuniform rational B-spline parameters. Unsteady, low speed laminar flows are computed using a Navier–Stokes solver in a parallel computing environment. The numerical evaluation of the gradient vector components, which requires unsteady flow solutions, is also performed in parallel. It is shown that the thrust generation may significantly be increased in comparison to the sinusoidal flapping motion. For a maximum thrust generation, the airfoil stays at about a constant angle of attack during the upstroke and the downstroke, and may reach very high effective angle of attack values. The pitching motion mostly occurs at the minimum and maximum plunge positions.

Nomenclature

C_d	=	drag coefficient
C_P	=	power coefficient
C_p	=	pressure coefficient
C_T	=	average thrust coefficient
c	=	airfoil chord length
$f(\omega t)$	=	nonsinusoidal nonuniform rational B-spline-based periodic function
h	=	plunge position
h_0	=	plunge amplitude
k	=	reduced frequency, $\omega c/U_\infty$
l	=	optimization step number
M	=	freestream Mach number
P_0, P_1, P_2	=	nonuniform rational B-spline parameters
Re	=	Reynolds number based on the chord length
T	=	period of a flapping motion
t	=	time
U_∞	=	freestream velocity
$\boldsymbol{V}$	=	velocity vector
α	=	pitch angle
α_0	=	pitch amplitude
β	=	weight of the efficiency in the objective function
η	=	propulsive efficiency
ϕ	=	phase shift between plunge and pitch motions
ω	=	angular frequency

I. Introduction

BASED on observations on flying birds, insects, and swimming fish, it appears that flapping wings may be favorable for flights of very small scale vehicles, so-called micro air vehicles (MAVs) with wingspans of 15 cm or less. The current interest in the research and development community is to find the most energy efficient airfoil adaptation and flapping-wing motion technologies capable of providing the required aerodynamic performance for a MAV flight.

Recent experimental and computational studies investigated the kinematics, dynamics, and flow characteristics of flapping wings, and shed some light on lift, drag, and propulsive power considerations [1,2]. In their experimental study, Lai and Platzer [3] investigate drag-producing wake flows and thrust-producing jetlike flows downstream of a plunging airfoil. Water tunnel flow visualization experiments by Jones et al. [4] provide a considerable amount of information on the wake characteristics of flapping airfoils. Another water tunnel study is conducted by Heatcote et al. [5] to observe the effect of spanwise flexibility on the thrust, lift, and propulsive efficiency of a rectangular wing in a pure plunge motion. They find that introducing a degree of spanwise flexibility is beneficial in terms of high thrust and propulsive efficiency. In their experiments, Anderson et al. [6] observe that the phase shift between pitch and plunge oscillations plays a significant role in maximizing propulsive efficiency. A recent experimental study by Schouveiler et al. [7] shows that high thrust and efficiency conditions can be achieved together for some range of flapping parameters.

Lewin and Haj-Hariri [8] examines the propulsive characteristics of an airfoil plunging sinusoidally over a range of frequencies and plunge amplitudes to correlate viscous flow structures to thrust generation. Hover et al. [9] use sinusoidal and nonsinusoidal effective angle of attack variations in time to investigate the propulsive performance of an airfoil undergoing combined plunge and pitch oscillations. Lee et al. [10] identify the key physical flow phenomenon dictating the thrust generation of a plunging and/or pitching airfoil in terms of flow and/or geometry parameters.

Navier–Stokes computations performed by Tuncer and Platzer [11] show that an airfoil undergoing combined pitch and plunge oscillations may produce high thrust at a high propulsive efficiency under certain kinematic conditions. Tuncer et al. [12,13] also observe that the thrust and the propulsive efficiency values may be significantly increased in the case of flapping/stationary airfoil combinations in tandem. Using a Navier–Stokes solver, Isogai et al. [14] explore the effect of dynamic stall phenomena on the thrust generation and the propulsive efficiency of flapping airfoils. Young and Lai [15] show that vortical wake structures, and the lift and thrust characteristics of a plunging airfoil are strongly dependent on the oscillation frequency and amplitude.

Jones and Platzer [16] recently demonstrated a radio-controlled micro air vehicle propelled by flapping wings in a biplane configuration. The experimental and numerical studies by Jones et al. [16–18] and Platzer and Jones [19] on flapping-wing propellers points at the gap between numerical flow solutions and the actual flight conditions over flapping wings.

In earlier studies [11,12], the average thrust coefficient of a NACA0012 airfoil flapping sinusoidally in combined plunge and pitch was obtained for a range of reduced frequencies and amplitudes of the flapping motion. Computational and experimental findings show that the thrust generation and the propulsive efficiency of flapping airfoils are closely related to the flapping motion and flow parameters. In a later study [20], the present authors employed a gradient based optimization of sinusoidal flapping motion parameters, such as the flapping frequency, the amplitude of pitch

Received 26 December 2006; accepted for publication 13 April 2007.

*Graduate Research Assistant, Department of Aerospace Engineering.
†Professor, Department of Aerospace Engineering. Member AIAA.

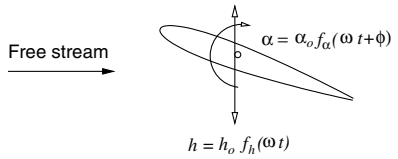

Fig. 1 Flapping motion of an airfoil.

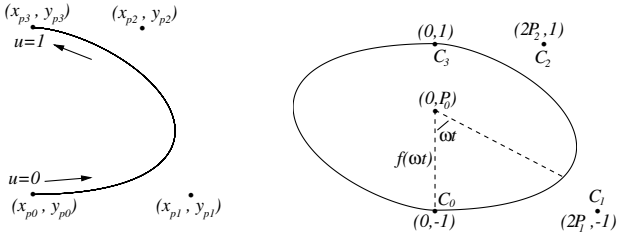

Fig. 2 Flapping path defined by a third degree NURBS.

and plunge motions, and the phase shift between them, to maximize the thrust and/or propulsive efficiency of flapping airfoils. It should be noted that in sinusoidal motion, pitch and plunge positions are based on the projection of a vector rotating on a unit circle, and maximum plunge and pitch velocities occur at mean plunge and pitch positions. In a following study [21], the sinusoidal periodic motion is relaxed by replacing the unit circle with an ellipse. The optimization of the flatness coefficient, which is the ratio of the axes of an ellipse, shows that the thrust generation of flapping airfoils may further be increased on an elliptic flapping path.

In the present study, the periodic flapping motion (Fig. 1) is further relaxed by using a closed curve defined by a third degree nonuniform rational B splines (NURBS, Fig. 2). The parameters defining the NURBS are then optimized for the maximum thrust and/or the propulsive efficiency.

II. Nonsinusoidal Periodic Path Based on NURBS

A smooth curve S based on a general nth degree rational Bezier segment is defined as follows [22]:

$$S(u) = [x(u), y(u)] = \frac{\sum_{i=0}^{n} W_i B_{i,n}(u) C_i}{\sum_{i=0}^{n} W_i B_{i,n}(u)} \qquad 0 \le u \le 1 \tag{1}$$

where $B_{i,n}(u) \equiv [n!/i!(n-i)!]u^i(1-u)^{n-i}$ are the classical nth degree Bernstein polynomials, and $C_i = (x_{pi}, y_{pi})$, are called control points with weights W_i. Note that $S(u=0) = C_0$ and $S(u=1) = C_n$. A closed curve which describes the upstroke and downstroke of a flapping path is then defined by employing a NURBS composed of two third degree rational Bezier segments. The control points and their corresponding weights are chosen such that the nonsinusoidal periodic function (y coordinates of the closed curve) is between -1 and 1. The periodic flapping motion is finally defined by three parameters. The first parameter P_0 defines the center of the rotation vector on the closed curve. The remaining two parameters P_1 and P_2 are used to define the x coordinates of the control points, which are $C_1 = (2P_1, -1)$ and $C_2 = (2P_2, 1)$ (Fig. 2). The parameters P_1 and P_2 define the flatness of the closed NURBS curve.

The x and y coordinates on the periodic NURBS curve may be obtained as a function of the parameter u:

$$\begin{aligned} x(u) &= \frac{2P_1 u(1-u)^2 + 2P_2 u^2(1-u)}{(1-u)^3 + u(1-u)^2 + u^2(1-u) + u^3} \\ y(u) &= \frac{-(1-u)^3 - u(1-u)^2 + u^2(1-u) + u^3}{(1-u)^3 + u(1-u)^2 + u^2(1-u) + u^3} \end{aligned} \tag{2}$$

The nonsinusoidal periodic function f is then defined as

$$f[u(\omega t)] = y(u) \equiv f(\omega t) \tag{3}$$

where

$$\tan(\omega t) = -\frac{x(u)}{y(u) - P_0} \tag{4}$$

For a given ωt position, Eq. (4) is solved for u. Once u is determined, $y(u) \equiv f(\omega t)$ is evaluated using Eq. (2).

III. Numerical Solution Method

Two-dimensional unsteady viscous flows around a flapping airfoil are computed by solving the Navier–Stokes equations on a moving C grid. The grid is partitioned into overlapping subgrids, and computations on subgrids are performed in parallel. A gradient based optimization is employed for the optimization of flapping motion parameters to maximize the average thrust coefficient and/or the propulsive efficiency.

A. Navier–Stokes Solver

The strong conservation-law form of the 2-D, thin-layer, Reynolds averaged Navier–Stokes equations is solved on each subgrid. The governing equations in a curvilinear coordinate system (ξ, ζ) are given as

$$\partial_t \hat{\mathbf{Q}} + \partial_\xi \hat{\mathbf{F}} + \partial_\zeta \hat{\mathbf{G}} = Re^{-1} \partial_\zeta \hat{\mathbf{S}} \tag{5}$$

where $\hat{\mathbf{Q}}$ is the vector of conservative variables, $\hat{\mathbf{F}}$ and $\hat{\mathbf{G}}$ are the convective flux vectors, and $\hat{\mathbf{S}}$ is the thin-layer approximation of the viscous fluxes in the ζ direction normal to the airfoil surface. The convective fluxes are evaluated using the third order accurate Osher's upwind biased flux difference splitting scheme. The discretized equations are solved by an approximately factored, implicit algorithm [11,12].

B. Boundary Conditions

The flapping motion of the airfoil is imposed by moving the airfoil and the C grid around it. The combined plunge h and pitch α motions of the airfoil are described by

$$h = -h_0 f_h(\omega t), \qquad \alpha = -\alpha_0 f_\alpha(\omega t + \phi) \tag{6}$$

where h_0 and α_0 are the plunge and pitch amplitudes, f is the periodic function based on NURBS, ω is the angular frequency which is given in terms of the reduced frequency, $k = (\omega c/U_\infty)$. ϕ is the phase shift between the plunging and the pitching motions. The pitch axis is located at the midchord.

At the overlapping boundaries of the subgrids, at every time step, the conservative flow variables are exchanged among the subgrids.

C. Effective Angle of Attack

An important parameter for analyzing the performance of the flapping airfoils is the instantaneous effective angle of attack. The effective angle of attack due to the pitching and plunging velocities at the leading edge is defined by

$$\alpha_{\text{eff}}(t) = \alpha(t) - \arctan\left(\frac{\dot{h}(t) + \frac{1}{2}c\dot{\alpha}(t)\cos[\alpha(t)]}{U_\infty - \frac{1}{2}c\dot{\alpha}(t)\sin[\alpha(t)]}\right) \tag{7}$$

where $\frac{1}{2}c$ is the distance between the leading edge and the pitch axis.

D. Optimization

The objective function is taken as a linear combination of the average thrust coefficient C_T and the propulsive efficiency η over a flapping period:

$$O^l[C_T, \eta] = (1-\beta)\frac{C_T^l}{C_T^{l-1}} + \beta\frac{\eta^l}{\eta^{l-1}} \tag{8}$$

The thrust coefficient is based on the integration of the drag coefficient over a flapping period. The propulsive efficiency is the ratio of the power extracted through thrust to the power input required to sustain the flapping motion:

Table 1 Optimization cases and initial conditions based on sinusoidal path optimization

Case	β	α_0	ϕ	P_{0h}	P_{1h}	P_{2h}	$P_{0\alpha}$	$P_{1\alpha}$	$P_{2\alpha}$	η	C_T
1	0.0	8.5 deg	90.3 deg	0	1	1	0	1	1	0.43	0.14
2	0.5	14.6 deg	89.7 deg	0	1	1	0	1	1	0.58	0.12
3	1.0	18.3 deg	81.5 deg	0	1	1	0	1	1	0.61	0.10

Table 2 Nonsinusoidal optimization results

Case	β	α_0	ϕ	P_{0h}	P_{1h}	P_{2h}	$P_{0\alpha}$	$P_{1\alpha}$	$P_{2\alpha}$	η	C_T
1	0.0	21.2 deg	41.4 deg	−0.9	3.5	4.4	−0.8	0.2	0.2	0.21	0.78
2	0.5	17.9 deg	80.8 deg	−0.4	1.3	1.6	−0.1	0.99	1	0.57	0.18
3	1.0	21.5 deg	79.9 deg	−0.1	1.02	1.01	−0.01	1	1	0.64	0.09

$$C_T = -\frac{1}{T}\int_t^{t+T} C_d \, \mathrm{d}t, \qquad \eta = \frac{C_T U_\infty}{C_P}$$
$$C_P = \frac{1}{T}\int_t^{t+T}\int_S C_p(\boldsymbol{V}\cdot \mathrm{d}\boldsymbol{A})\,\mathrm{d}t \tag{9}$$

where T is the period of the flapping motion. C_P is the power coefficient which accounts for the rate of average work required to maintain the flapping motion. It should be noted that the mass, therefore the inertia of the airfoil is ignored in the evaluation of the power coefficient. l denotes the iteration step during the optimization process. Note that $\beta = 0$ sets the objective function to the normalized thrust coefficient.

A gradient based optimization process is employed. The gradient vector of the objective function ∇O provides the direction of the steepest ascent, along which the objective function has the maximum rate of change:

$$\nabla O(\boldsymbol{V}) = \frac{\partial O}{\partial V_1}\boldsymbol{v}_1 + \frac{\partial O}{\partial V_2}\boldsymbol{v}_2 + \cdots \tag{10}$$

where V_i's are the optimization variables, and the $\boldsymbol{v}_i$'s are the corresponding unit vectors in the variable space.

The components of the gradient vector are then evaluated numerically by computing the objective function for a perturbation of all the optimization variables one at a time. It should be noted that the evaluation of these vector components requires an unsteady flow solution over a few periods of the flapping motion until a periodic flow behavior is reached. Once the unit gradient vector is evaluated, an optimization step $\Delta \boldsymbol{S} = \varepsilon \frac{\nabla O}{|\nabla O|}$ is taken along the vector. This process continues until a local maximum in the optimization space is reached. The step size ε is evaluated by a line search along the gradient vector, at every optimization step.

In the optimization studies, the flatness of the NURBS curve may be constrained through P_1 and P_2 parameters to exclude curves with large curvatures, which indicate the regions of large accelerations along the flapping path. Similarly the center of rotation P_0 may also be constrained to prevent very large accelerations along a periodic motion.

E. Parallel Processing

In the solution of unsteady flows, a parallel algorithm based on domain decomposition is implemented in a master-worker paradigm. The C grid is partitioned into overlapping subgrids first, and the solution on each subgrid is computed as a separate process in the computer cluster. The flow variables at the overlapping subgrid boundaries are exchanged among the subgrid processes at each time step of the unsteady solution. PVM (version 3.4.5) library routines are used for interprocess communication. In the optimization process, the components of the gradient vector which require unsteady flow solutions with perturbed optimization variables, are also computed in parallel. Computations are performed in a cluster of Linux based computers with dual Xeon and Pentium-D processors.

IV. Results and Discussion

In this optimization study, the optimization variables are chosen as the NURBS parameters defining the plunging and pitching paths P_{0h}, P_{1h}, P_{2h}, $P_{0\alpha}$, $P_{1\alpha}$, and $P_{2\alpha}$ (Fig. 2), the phase shift between the pitch

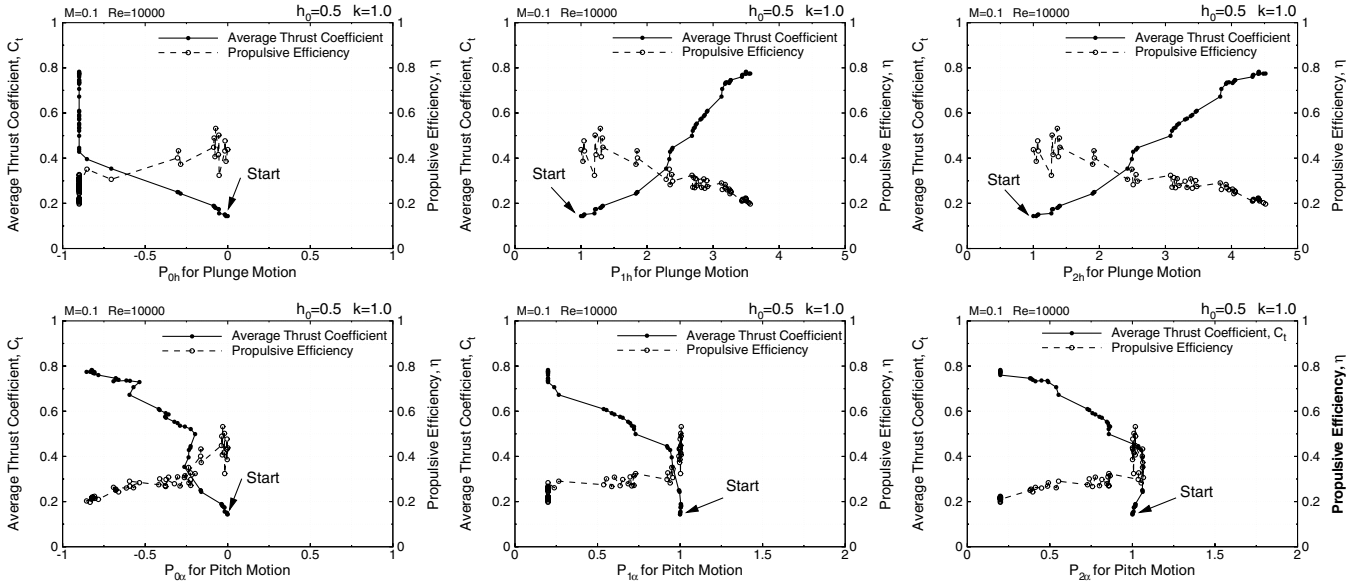

Fig. 3 Optimization steps for case 1.

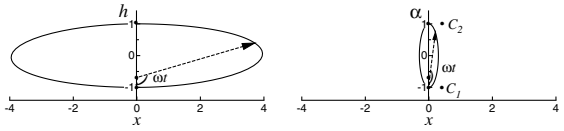

Fig. 4 NURBS curves defining plunge and pitch motions in case 1.

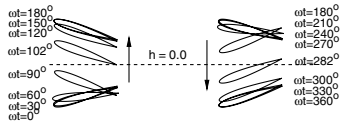

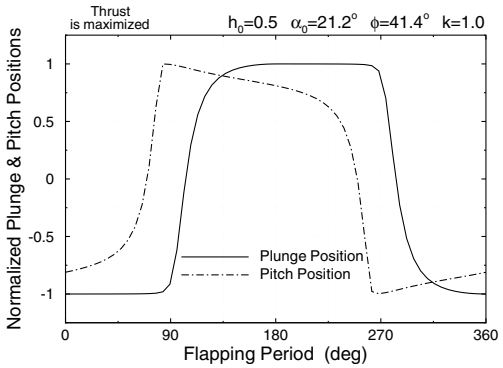

Fig. 5 Nonsinusoidal flapping motion for case 1.

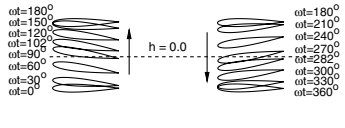

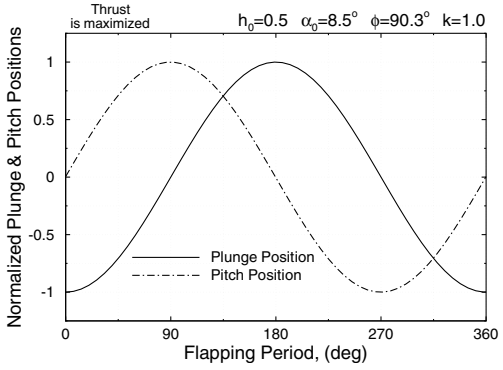

Fig. 6 Sinusoidal flapping motion for case 1.

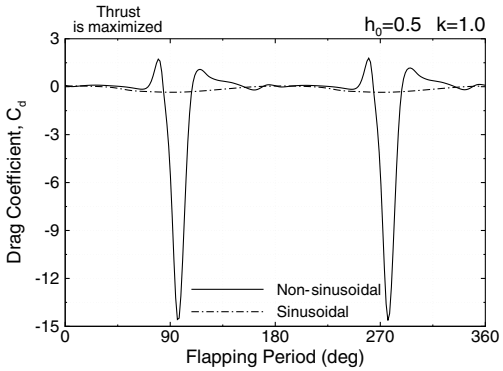

Fig. 7 Unsteady drag coefficient for case 1.

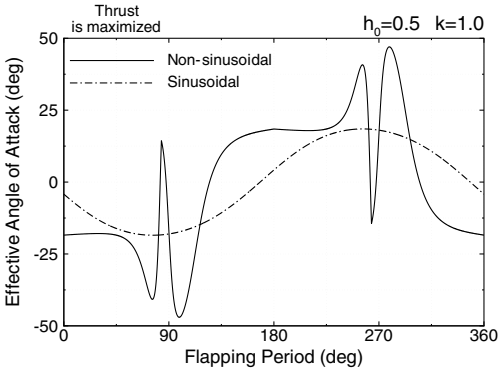

Fig. 8 Unsteady effective angle of attack for case 1.

h_0=0.5 α_0=21.2° ϕ=41.4°
P_{0h}=-0.90 P_{1h}=3.50 P_{2h}=4.42
$P_{0\alpha}$=-0.82 $P_{1\alpha}$=0.20 $P_{2\alpha}$=0.20

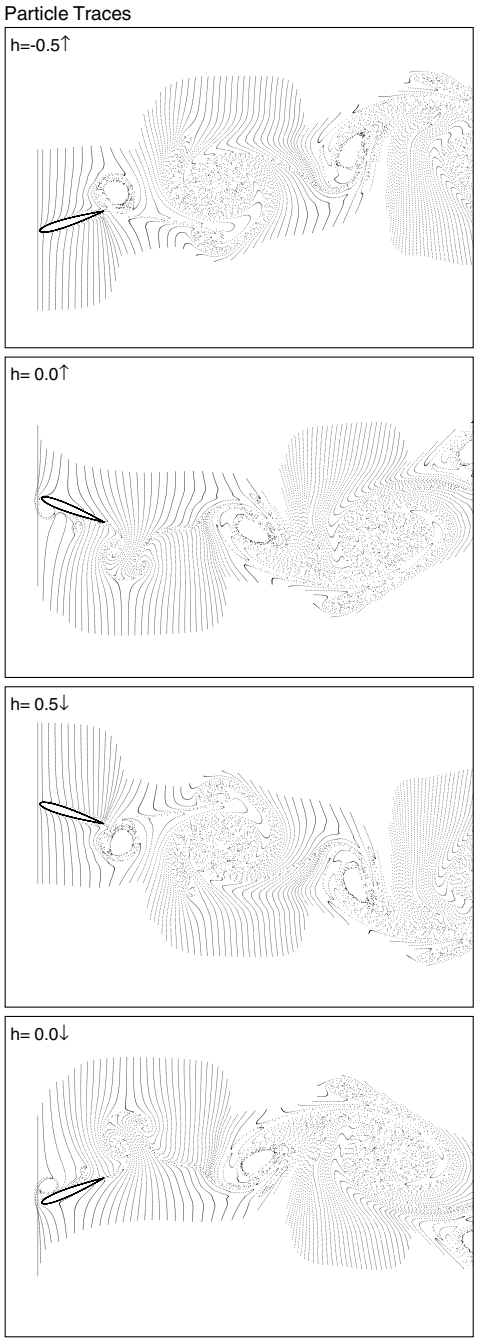

Fig. 9 The unsteady flowfield for nonsinusoidal flapping motion in case 1.

and plunge motions ϕ, and the pitch amplitude α_0. As the airfoil is set to a flapping motion in plunge and pitch on a closed path defined by NURBS, the NURBS parameters are optimized for maximum thrust and/or propulsive efficiency.

The optimization variables are optimized for fixed values of the reduced flapping frequency $k \equiv (\omega c/U_\infty) = 1.0$ and the plunge amplitude $h_0 = 0.5$. The unsteady laminar flowfields are computed at a low Mach number of 0.1 and a Reynolds number of 10,000. In a typical optimization process, parallel computations take about 30–100 h of wall clock time using 10–16 Pentium 4, 2.4 GHz processors. Flowfields are analyzed in terms of unsteady particle traces, variations of the unsteady thrust/drag coefficient, and effective angle of attack in a flapping period. Particle traces are obtained by a simple and efficient integration of the particle path lines within the flow solver as the unsteady flowfield is computed.

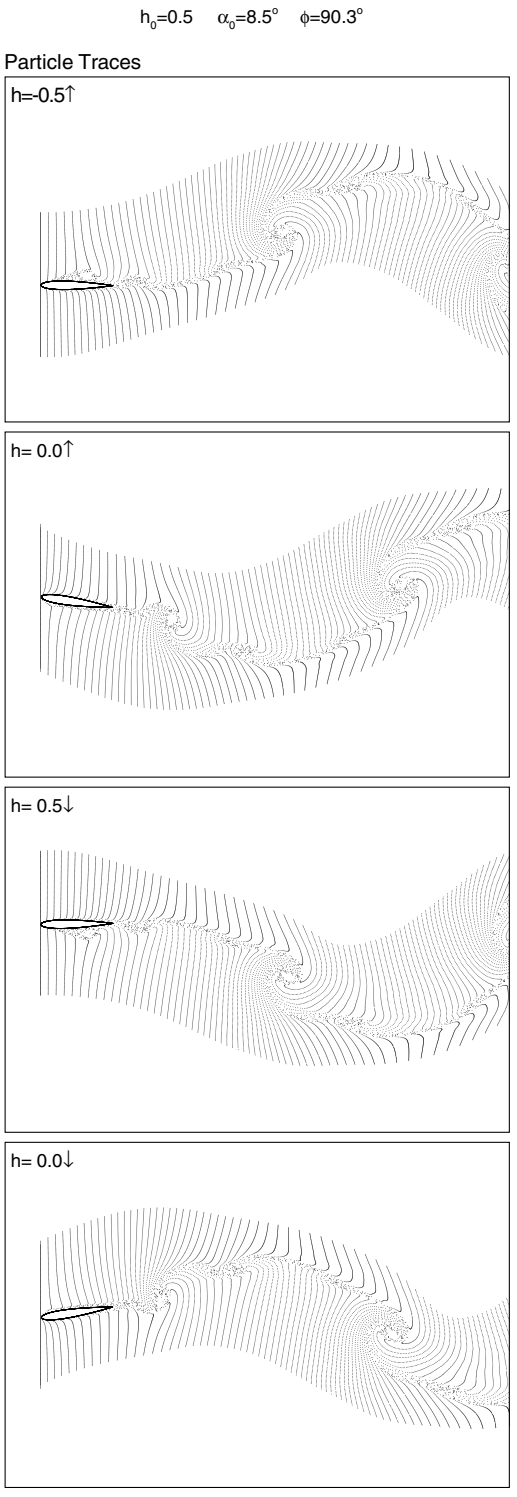

Fig. 10 The unsteady flowfield for sinusoidal flapping motion in case 1.

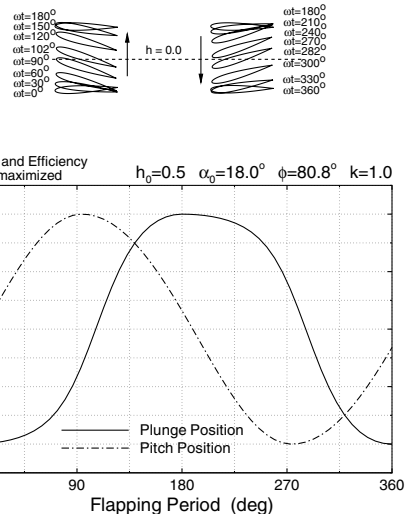

Fig. 11 Nonsinusoidal flapping motion for case 2.

In this study, the P_1 and P_2 values are constrained within the range 0.2 to 5.0, and P_0 in the range -0.9 to 0.9, to define a proper flapping motion which does not impose excessively large accelerations. A flapping motion with very large instantaneous accelerations causes numerical difficulties in reaching periodic flow solutions, and is, in fact, not practical due to the inertial effects.

The optimization cases studied and the initial conditions are given in Table 1. The initial values of the optimization variables correspond to the optimum sinusoidal flapping motion for the given β value, which are obtained from an optimization study [21]. It should be noted that the NURBS parameters in the initial conditions define a sinusoidal flapping motion. The nonsinusoidal optimization results obtained in this study are given in Table 2.

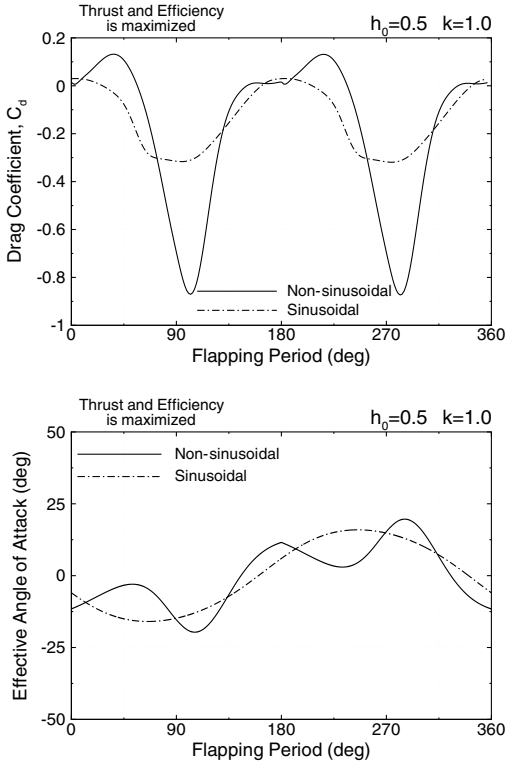

Fig. 12 Unsteady drag coefficient and effective angle of attack for case 2.

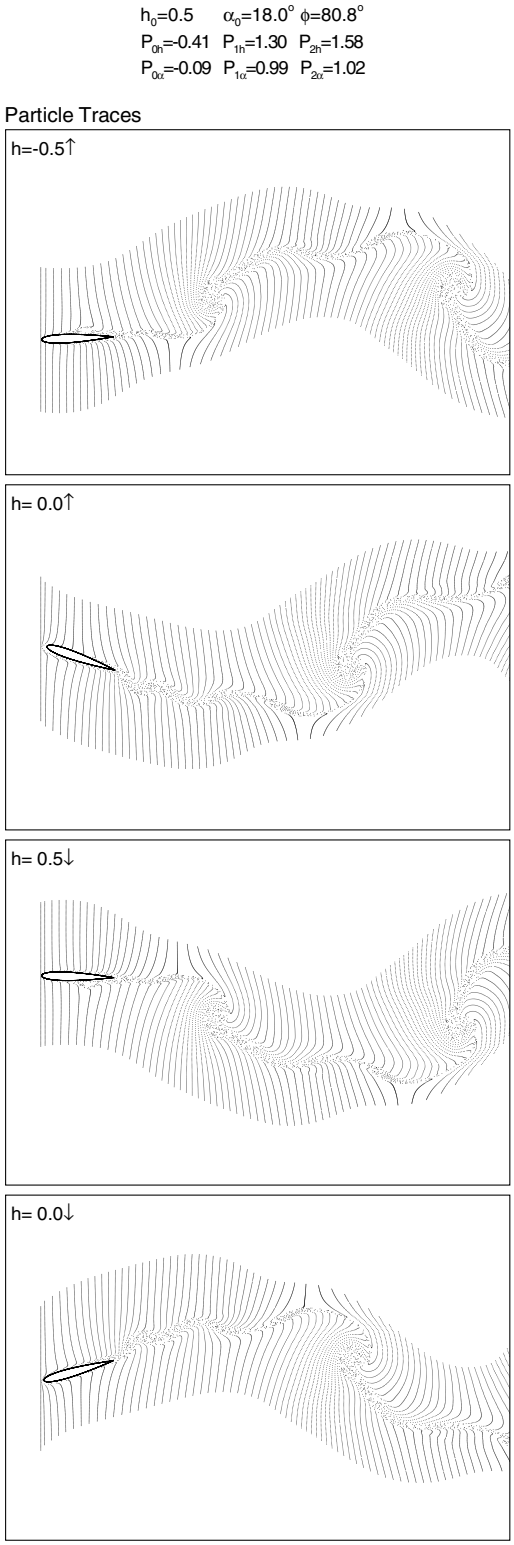

Fig. 13 The unsteady flowfield for nonsinusoidal flapping motion in case 2.

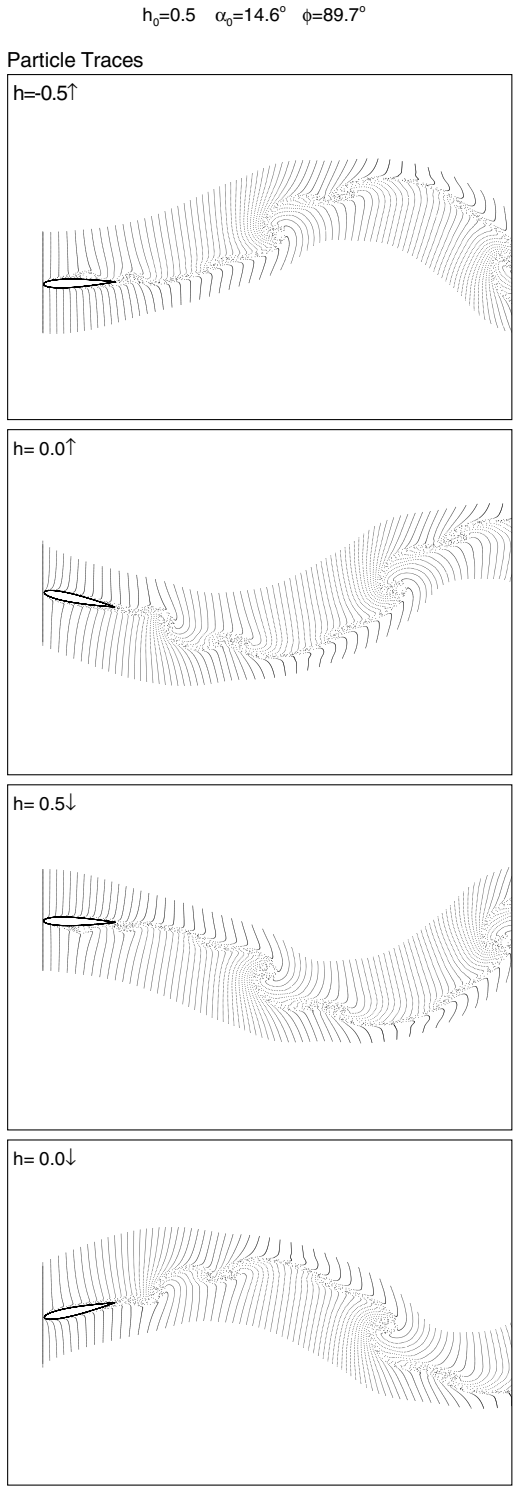

Fig. 14 The unsteady flowfield for sinusoidal flapping motion in case 2.

The variation of NURBS parameters along the optimization steps for case 1 are shown in Fig. 3. As all the optimization variables are incremented in the direction of the gradient vector, the average thrust coefficient increases gradually from $C_T = 0.14$, which is the maximum value for the sinusoidal flapping motion, and reaches a maximum value of $C_T = 0.78$. The corresponding propulsive efficiency is about 21% in contrast to the starting value of $\eta = 43\%$.

The NURBS curves defined by the optimized parameters and the centers of rotation vectors, which together define the nonsinusoidal plunge and pitch motions, are given in Fig. 4. The corresponding optimum nonsinusoidal flapping motion is given in Fig. 5 in comparison to the optimum sinusoidal flapping motion (Fig. 6). It is noted that the nonsinusoidal flapping motion differs significantly from the sinusoidal motion. The pitching motion now mostly occurs at the minimum and maximum plunge positions, and the airfoil stays at about a constant incidence angle during the up and down strokes. Figures 7 and 8 show the corresponding drag coefficient and the effective angle of attack variations in time, respectively. As the airfoil pitches up at the bottom plunge position, the effective angle of attack decreases rapidly due to the pitch rate. As the angle of attack increases, the pitch rate decreases and the effective angle of attack

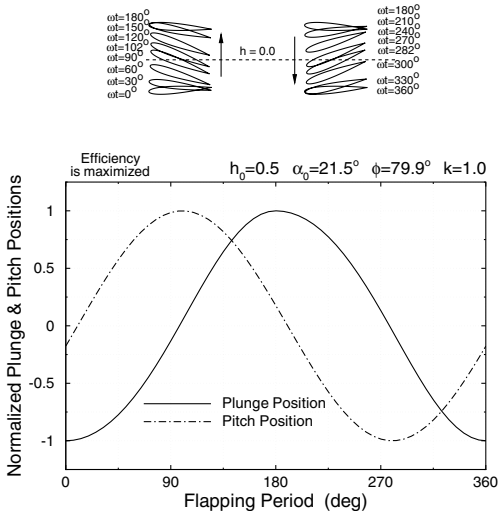

Fig. 15 Nonsinusoidal flapping motion for case 3.

becomes positive. Along this pitching process the airfoil produces the first drag peak. The following rapid plunging motion upward at about a constant angle of attack produces minimum drag/maximum thrust peak observed. As the airfoil reaches the top plunge position, the plunge and pitch rates diminish. The airfoil then sees a positive effective angle of attack, and again produces the second drag peak. The same process repeats in reverse as the airfoil undergoes the downstroke. Such a nonsinusoidal flapping motion produces very high effective angle of attack values for short durations about midplunge positions, and causes a much higher thrust production. The overall thrust production is about 5 times higher than that of the sinusoidal flapping motion.

The nonsinusoidal and sinusoidal unsteady flowfields for case 1 are depicted in Figs. 9 and 10 in terms of particle traces. Particles are shed along a vertical line at the leading edge of the airfoil. As seen in the figures, the optimum nonsinusoidal flapping motion produces a highly vortical flowfield where the strong leading edge vortices are formed during the upstroke and the downstroke, and are shed into the wake, whereas the vortices generated in the optimum sinusoidal flapping motion are observed to be weaker.

In case 1, the thrust is maximized at a relatively low efficiency. In case 2, the thrust and the propulsive efficiency are optimized simultaneously by setting $\beta = 0.5$, which sets the objective function as a linear combination of the average thrust coefficient and the propulsive efficiency with equal weights. As seen in Table 2, the nonsinusoidal flapping motion based on NURBS produces about

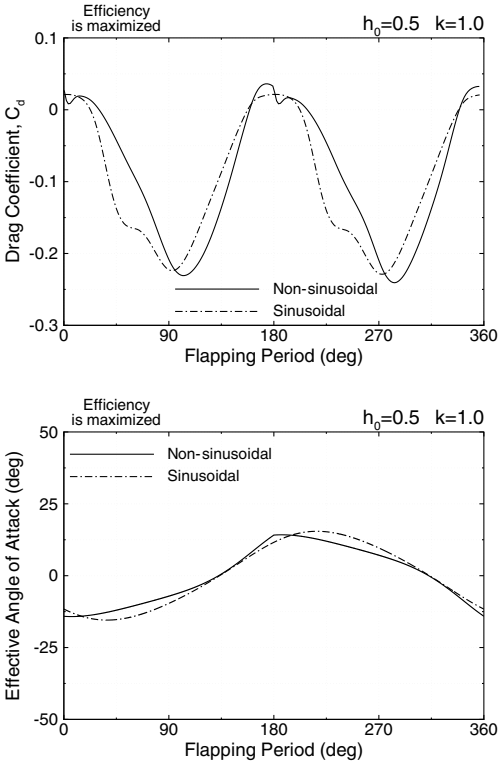

Fig. 16 Unsteady drag coefficient and effective angle of attack for case 3.

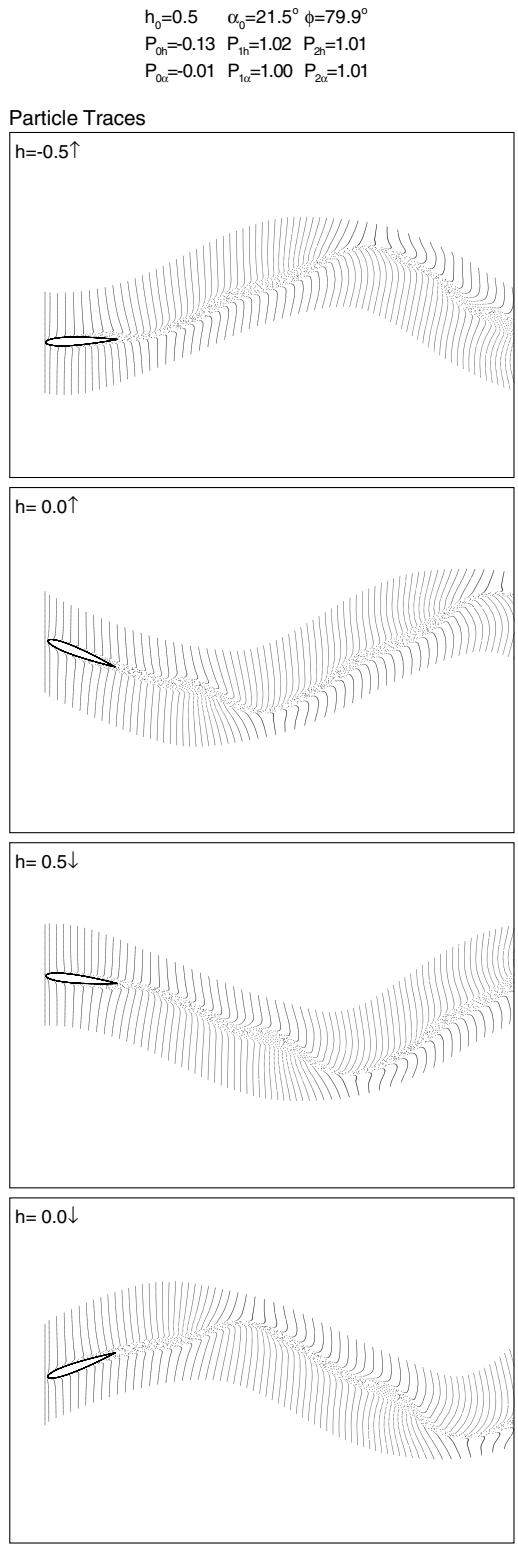

Fig. 17 The unsteady flowfield for nonsinusoidal flapping motion in case 3.

50% higher thrust than the sinusoidal motion without much of a loss in the propulsive efficiency. The optimized flapping motion, the unsteady variations of the drag coefficient, and the effective angle of attack are given in Figs. 11 and 12. The nonsinusoidal flapping motion again deviates from the sinusoidal motion. The airfoil similarly tends to stay longer at minimum and maximum plunge positions, and reaches higher plunge velocities around the midplunge positions. The peak thrust values reached are similarly much higher than the ones for sinusoidal flapping as observed in case 1. Instantaneous flowfields for both nonsinusoidal and sinusoidal flapping paths are given in Figs. 13 and 14, respectively. The leading edge vortices in both cases are observed to be not as strong as the ones in case 1. Consequently the flowfields are less vortical.

In case 3, where the propulsive efficiency is maximized, the optimum nonsinusoidal flapping motion based on NURBS does not significantly deviate from the sinusoidal motion (Fig. 15). It appears that the sinusoidal motion provides the best efficiency without producing much thrust. Time variations of the drag coefficient and the effective angle of attack are given in Fig. 16. The particle traces given in Fig. 17 shows that the unsteady flowfield is free of large vortical structures which apparently detrimental to the propulsive efficiency.

V. Conclusions

In this study, the flapping motion of an airfoil is defined by a third degree NURBS. The NURBS parameters are successfully optimized for maximum thrust and/or efficiency using a gradient based optimization and an unsteady Navier–Stokes solver. The study shows that the thrust generation of a flapping airfoil on a nonsinusoidal flapping path may be increased significantly in comparison to the sinusoidal flapping. However it is achieved at very high acceleration rates in both pitch and plunge, and at the expense of the propulsive efficiency. The nonsinusoidal flapping motion for maximum thrust imposes a plunging motion with an almost constant incidence angle during the upstroke and the downstroke while pitching occurs rapidly at the minimum and maximum plunge amplitudes. The thrust-producing flows are observed to be highly vortical with the formation of strong leading edge vortices during upstroke and the downstroke. Propulsive efficiency improves as the flapping path approaches a sinusoidal one.

Acknowledgment

The present work was partially supported by Middle East Technical University under Projects No. BAP-2006.03.13.01 and No. BAP-2002.03.13.04.

References

[1] Mueller, T. J. (ed.), *Fixed and Flapping Wing Aerodynamics for Micro Air Vehicles*, Vol. 195, Progress in Aeronautics and Astronautics, AIAA, Reston, VA, 2001.

[2] Shyy, W., Berg, M., and Lyungvist, D., "Flapping and Flexible Wings for Biological and Micro Air Vehicles," *Progress in Aerospace Sciences*, Vol. 35, No. 5, 1999, pp. 455–505.

[3] Lai, J. C. S., and Platzer, M. F., "Jet Characteristics of a Plunging Airfoil," *AIAA Journal*, Vol. 37, No. 12, 1999, pp. 1529–1537.

[4] Jones, K. D., Dohring, C. M., and Platzer, M. F., "Experimental and Computational Investigation of the Knoller–Beltz Effect," *AIAA Journal*, Vol. 36, No. 7, 1998, pp. 1240–1246.

[5] Heatcote, S., Wang, Z., and Gursul, I., "Effect of Spanwise Flexibility on Flapping Wing Propulsion," AIAA Paper 2006-2870, June 2006.

[6] Anderson, J. M., Streitlen, K., Barrett, D. S., and Triantafyllou, M. S., "Oscillating Foils of High Propulsive Efficiency," *Journal of Fluid Mechanics*, Vol. 360, Apr. 1998, pp. 41–72.

[7] Schouveiler, L., Hover, F. S., and Triantafyllou, M. S., "Performance of Flapping Foil Propulsion," *Journal of Fluids and Structures*, Vol. 20, No. 7, Special Issue, 2005, pp. 949–959.

[8] Lewin, G. C., and Haj-Hariri, H., "Modelling Thrust Generation of a Two-Dimensional Heaving Airfoil in a Viscous Flow," *Journal of Fluid Mechanics*, Vol. 492, Oct. 2003, pp. 339–362.

[9] Hover, F. S., Haugsdal, Ø., and Triantafyllou, M. S., "Effect of Angle of Attack Profiles in Flapping Foil Propulsion," *Journal of Fluids and Structures*, Vol. 19, No. 1, 2004, pp. 37–47.

[10] Lee, J.-S., Kim, C., and Kim, K. H., "Design of Flapping Airfoil for Optimal Aerodynamic Performance in Low-Reynolds Number Flows," *AIAA Journal*, Vol. 44, No. 9, 2006, pp. 1960–1972.

[11] Tuncer, I. H., and Platzer, M. F., "Computational Study of Flapping Airfoil Aerodynamics," *Journal of Aircraft*, Vol. 37, No. 3, 2000, pp. 514–520.

[12] Tuncer, I. H., and Platzer, M. F., "Thrust Generation due to Airfoil Flapping," *AIAA Journal*, Vol. 34, No. 2, 1996, pp. 324–331.

[13] Tuncer, I. H., Lai, J., Ortiz, M. A., and Platzer, M. F., "Unsteady Aerodynamics of Stationary/Flapping Airfoil Combination in Tandem," AIAA Paper 1997-659, Jan. 1997.

[14] Isogai, K., Shinmoto, Y., Watanabe, Y., "Effects of Dynamic Stall on Propulsive Efficiency and Thrust of a Flapping Airfoil," *AIAA Journal*, Vol. 37, No. 10, 1999, pp. 1145–1151.

[15] Young, J., and Lai, J. C. S., "Oscillation Frequency and Amplitude Effects on the Wake of a Plunging Airfoil," *AIAA Journal*, Vol. 42, No. 10, 2004, pp. 2042–2052.

[16] Jones, K. D., and Platzer, M. F., "Experimental Investigation of the Aerodynamic Characteristics of Flapping-Wing Micro Air Vehicles," AIAA Paper 2003-418, Jan. 2003.

[17] Jones, K. D., Castro, B. M., Mahmoud, O., Pollard, S. J., Platzer, M. F., Neef, M. F., Gonet, K., and Hummel, D., "A Collaborative Numerical and Experimental Investigation of Flapping-Wing Propulsion," AIAA Paper 2002-706, Jan. 2002.

[18] Jones, K. D., Duggan, S. J., and Platzer, M. F., "Flapping-Wing Propulsion for a Micro Air Vehicle," AIAA Paper 2001-126, Jan. 2001.

[19] Platzer, M. F., and Jones, K. D., "The Unsteady Aerodynamics of Flapping-Foil Propellers," *Proceedings of the 9th International Symposium on Unsteady Aerodynamics, Aeroacoustics and Aero-elasticity of Turbomachines*, edited by P. Ferrand and S. Aubert, Presses Universitaires de Grenoble, Grenoble, France, 2001, pp. 123–147.

[20] Tuncer, I. H., and Kaya, M., "Optimization of Flapping Airfoils For Maximum Thrust and Propulsive Efficiency," *AIAA Journal*, Vol. 43, No. 11, 2005, pp. 2329–2341.

[21] Kaya, M. and Tuncer, I. H., "Path Optimization of Flapping Airfoils for Maximum Thrust Based on Unsteady Viscous Flow Solutions," *Proceedings of the 3rd Ankara International Aerospace Conference* [CD-ROM], Middle East Technical University, Ankara, Turkey, 2005; Paper No. AIAC-2005-011.

[22] Piegl, L., and Tiller, W., *The NURBS Book*, 2nd ed., Springer–Verlag, Berlin, 1997, Chap. 4.

J. Samareh
Associate Editor